Biophysical Chemistry, 48 (1993) 241–257
Elsevier Science Publishers B.V., Amsterdam

BIOCHE 01795

Fluorescence depletion measurements in various experimental geometries provide true emission and absorption anisotropies for the study of protein rotation

Thomas R. Londo [1], Noorul A. Rahman [1], Deborah A. Roess and B. George Barisas *

Departments of Chemistry and Physiology, Colorado State University, Fort Collins, CO 80523 (USA)

(Received 26 April 1993; accepted in revised form 6 July 1993)

Abstract

Use of fluorescence depletion methods for measuring slow protein rotational diffusion has been limited by failure to obtain, from depletion data, well-defined anisotropy functions dependent on the distribution of either fluorophore emission or absorption transition dipoles, but not both. Such anisotropies would be directly comparable to those obtained from phosphorescence emission or triplet absorption measurements. We now describe such procedures applicable to cuvet and microscope experimental geometries, together with supporting experimental results. In cuvet measurements, the pump and probe beams are colinear and fluorescence is collected at 90° to this axis. The data analysis procedure for this geometry has been suggested by Wegener (*Biophys. J.*, 46 (1984) 795) and permits calculation of the absorption and emission anisotropies and the interdipole angle. In microscope experiments, fluorescence emission is collected along the pump/probe beam axis. For microscope measurements, a new experimental procedure permits evaluation of absorption and emission anisotropies when the interdipole angle is independently known. In either case multiple depletion measurements are required, each with different relative orientations of the probe beam polarization, pump beam polarization and emission polarizer axis. We have used these methods to calculate the time-dependent anisotropies for eosin-derivatized BSA rotation in glycerol solutions in both experimental geometries. These data correspond well with those obtained from time-resolved phosphorescence anisotropy measurements.

Keywords: Rotation; Protein; Fluorescence depletion; Anisotropy

1. Introduction

Integral membrane proteins play important roles in cellular activation, adhesion, metabolism, transport and locomotion [1–3]. A major research interest of our group is understanding how

* Corresponding author.
[1] Present address: Hybritech, Incorporated, La Jolla, California 92196, USA.

Abbreviations used: RCT, rotational correlation time; TPA, time-resolved phosphorescence anisotropy; ErITC, erythrosin isothiocyanate; EITC, eosin isothiocyanate; BSA, ovine serum albumin; PFD, polarized fluorescence depletion.

changes in the motions of such proteins reflect and/or modulate primary events in cellular activation. In particular, rates of rotational diffusion [4] are sensitive measures of the size and microenvironment of these molecules. Experimentally, rotational diffusion is quantitated through the time decay of functions like the emission anisotropy of probe chromophores attached to a membrane protein. A useful parameter derived from such analyses is the rotational correlation time [5] (RCT), a quantity proportional both to the in-membrane volume of the protein and to the membrane viscosity. Although various methods have been developed to measure rotational correlation times of cell membrane proteins [6–8], only two of these are of broad and general applicability.

The older of these methods is time-resolved phosphorescence anisotropy (TPA), particularly as employed by Jovin and collaborators [9]. Phosphorescent probes like erythrosin isothiocyanate (ErITC) are excited by a few-nanosecond pulse of vertically polarized light. Phosphorescence is detected at 90° through an emission analyzer positioned alternatively vertically and horizontally. These polarized emission signals decay by triplet decay on the hundreds of microseconds to millisecond timescale [10] and by rotational relaxation of the probe-bearing macromolecules on the tens to hundreds of microsecond timescale. An appropriate combination of vertically and horizontally polarized intensities yields a signal, the intensity function, dependent only on the number of triplet excited states. Similarly, another combination, the phosphorescence anisotropy, reflects only the evolution of orientational asymmetry in the sample.

The other, more recent method, introduced by Garland and Johnson [11,12] as a microscope-based technique, is termed by us polarized fluorescence depletion [13–16] (PFD). This technique combines the long lifetimes of molecular triplet states with the sensitivity of fluorescence detection to measure protein rotational diffusion over the same timescale as TPA but with over 1000-fold greater sensitivity. This increase in sensitivity permits examination of protein rotation on microscopically selected individual cells. The method depends upon fluorophores like eosin isothiocyanate (EITC) which have substantial quantum yields both for triplet formation and for prompt fluorescence [17]. Rotationally mobile macromolecules labeled with such a chromophore are irradiated by a low intensity, linearly polarized probe beam. The resulting steady-state fluorescence is proportional to the number of ground state chromophores whose absorption transition dipoles are parallel to the probe polarization. The sample is then subjected to a brief pulse of high intensity, linearly polarized light. As a result of this pulse, a substantial fraction of chromophores undergo intersystem crossing to the triplet state. These triplets can exist for several hundred microseconds and, during this period, they cannot be excited to fluorescence by the probe beam. Thus, immediately after the pump pulse, there is a depletion in sample fluorescence which recovers back to the original steady state by the mechanisms of triplet decay and rotational reorientation.

The fundamental parameter characterizing molecular rotational diffusion is the time-dependent anisotropy function which establishes the rotational correlation time and, hence, the rotational diffusion coefficient of the rotating species [18]. For emission experiments the anisotropy function is simply calculated from observed emission intensities as $r(t) = (I(t)_{\parallel} - I(t)_{\perp})/(I(t)_{\parallel} + 2I(t)_{\perp})$. On the other hand the calculation of well-defined anisotropies from pump-probe experiments is complex. Smith et al. derived equations to calculate anisotropy functions obtained from polarized photobleaching signals gathered on a microscope-based instrument [19]. In their theory, however, they considered the case where the absorption transition dipole is *parallel* to the emission transition dipole. Axelrod also dealt with such signals measured in a microscope [20]. His treatment relaxed the constraint that the transition dipoles be parallel but omitted explicit relations between measured signals and anisotropy functions. Other groups have presented theories for obtaining absorption and emission anisotropies from PFD data using non microscope-based instrumentation [21–24]. Of particular interest is that described by Wegener [25] and

Wegener and Rigler [26]. They suggest a method using "magic-angle" orientations of various polarization axes to obtain anisotropy information from pairs of intensity measurements in four experimental geometries. We have recently modified our cuvet PFD apparatus to operate in this configuration. However, this experimental geometry cannot be realized in a microscope. In this paper, we describe a rigorous treatment of signals that *are* obtainable in a microscope to yield both absorption and emission anisotropy functions given the angle between the absorption and emission transition dipoles.

2. Theory

2.1. General treatment

The concept and experimental methods of PFD have been discussed in previous publications from this laboratory. The following development shows how these previous methods can be modified to obtain true emission and absorption anisotropies. We assume that a fluorophore is placed at the origin of an x, y, z laboratory coordinate system as illustrated in Fig. 1. The pump beam can, without loss of generality, be assumed to propagate along the x-direction and to be polarized in the z-direction. The probe beam also propagates along the x-axis and its polarization vector $\boldsymbol{a}$ makes an angle α with the z-axis. The various mathematical symbols used in this paper are summarized in the Glossary. We denote cos α as $\boldsymbol{a}\cdot\boldsymbol{z}$ and sin α as $[1-(\boldsymbol{a}\cdot\boldsymbol{z})^2]^{1/2}$. An emission polarizer is placed either parallel to the x-axis (in the microscope case) or parallel to the y-axis (in the 90° case) and its polarization vector $\boldsymbol{e}$ makes an angle ξ relative to the z-axis. We represent cos ξ as $\boldsymbol{e}\cdot\boldsymbol{z}$ and sin ξ as $[1-(\boldsymbol{e}\cdot\boldsymbol{z})^2]$. The azimuthal angle between the $\boldsymbol{a}$ and $\boldsymbol{e}$ vectors is defined as ϵ. The fluorescent probe contains an absorption transition dipole μ_a whose orientation is defined by the angles θ and ϕ. The probe also possesses an emission transition dipole μ_e which makes a fixed angle λ relative to μ_a. The emission dipole's orientation is defined by θ' and ϕ'. We also define the angle δ as the azimuthal angle between μ_a and μ_e. From this, we see that $\phi' = \phi + \delta$. These relations are depicted in Fig. 1. In what follows, we assume that $|\mu_a| = |\mu_e| = 1$, that these entities are fixed relative to the body of the fluorophore, and that the rotational dynamics are not altered upon excitation of the fluorophore. In addition, as discussed by Aragon and Pecora [27,28], we assume that the pump pulse is short in relation to the rotational correlation time of the sample.

We consider a distribution $W(\theta, \phi, \theta', \phi')$ of ground-state chromophores whose orientations

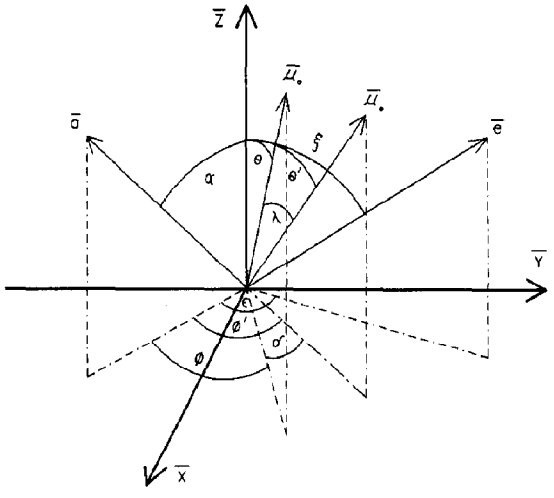

Fig. 1. Definition of vectors and angles used in derivations. A cell being examined lies at the origin of the coordinate system. See text for explanations of various quantities.

are defined by the orientations of their absorption and emission dipoles [29]. The orientational asymmetries of this distribution are quantitated by the emission and absorption anisotropy functions r_e and r_a, respectively. These quantities are defined by

$$r_a = \langle P_2(\boldsymbol{\mu}_a \cdot \boldsymbol{a})\rangle_d \tag{1}$$

$$r_e = \langle P_2(\boldsymbol{\mu}_e \cdot \boldsymbol{e})\rangle_d \tag{2}$$

where the $\langle \cdot \rangle_d$ denotes an average over the *difference* between the chromophore distribution before the pump pulse and some time thereafter, i.e. the ground state *depletion*. Actual depletion data consist of fluorescence recovery traces observed for specific sets of pump, probe and emission polarizer orientations. These signals normally depend on *both* the absorption *and* emission transition dipole distributions. Our initial goal is to find combinations of these signals, or signals obtained in unusual geometries, that depend on *only* the absorption or the emission transition dipole distribution *but not both*.

The probability for excitation of a given chromophore in this distribution by the probe beam is proportional to $(\boldsymbol{a} \cdot \boldsymbol{\mu}_a)^2$, while the probability for emission of a photon along $\boldsymbol{e}$ is proportional to $(\boldsymbol{e} \cdot \boldsymbol{\mu}_e)^2$. Given that the fraction of ground state chromophores excited in any given pulse is small, the distribution function for a ground state chromophore immediately after depletion is given by

$$S_0 = \frac{1}{4\pi}\left[1 - \frac{B}{3}P_0(\cos\theta) - \frac{2B}{3}P_2(\cos\theta)\right] \tag{3}$$

where $B/3$ is the total fractional ground state depletion and P_0 and P_2 are the zero and second order Legendre polynomials, respectively. For an excitation pulse that is short in comparison to both the triplet lifetime and the rotational relaxation time, $B/3$ is given by

$$\frac{B}{3} = \frac{2303 I_p \lambda_p \epsilon_M^p \Phi_t \Delta t}{hcN} \tag{4}$$

where I_p is the intensity of the depletion pulse, λ_p is the wavelength of light of the pump beam, ϵ_M^p is the molar absorptivity of the fluorophore for the pump beam, Φ_t is the quantum yield for triplet formation, N is Avogadro's number, c is the speed of light, h is Planck's constant, and Δt is the duration of the depletion pulse.

The fluorescence signals I observed in depletion experiments are given by

$$I = 3I_0\langle(\boldsymbol{a} \cdot \boldsymbol{\mu}_a)^2(\boldsymbol{e} \cdot \boldsymbol{\mu}_e)^2\rangle \tag{5}$$

where the angled brackets denote an average over the absorption and emission dipole distribution function. In turn, I_0 is given by

$$I_0 = \frac{2303\epsilon_M^a I_a \Phi_f E_f \lambda_a n}{N\lambda_e} \tag{6}$$

where ϵ_M^a is the molar absorptivity of the fluorophore for the probe beam, I_a is the intensity of the probe beam, Φ_f is the quantum yield for fluorescence, E_f is the detector efficiency, λ_a is the probe beam wavelength, λ_e is the fluorescence emission wavelength and n is the total number of chromophores illuminated.

From Fig. 1 and the spherical trigonometric identity for the cosine of the angle between two arbitrary vectors in three-dimensional space, we see that

$$\begin{aligned}(\boldsymbol{a} \cdot \boldsymbol{\mu}_a)^2 &= (\boldsymbol{a} \cdot \boldsymbol{z})^2 \cos^2\theta + \left[1 - (\boldsymbol{a} \cdot \boldsymbol{z})^2\right] \sin^2\theta \cos^2\phi \\ &\quad + 2(\boldsymbol{a} \cdot \boldsymbol{z})\left[1 - (\boldsymbol{a} \cdot \boldsymbol{z})^2\right]^{1/2} \cos\theta \sin\theta \cos\phi\end{aligned} \tag{7}$$

and that

$$\begin{aligned}(\boldsymbol{e} \cdot \boldsymbol{\mu}_e)^2 &= (\boldsymbol{e} \cdot \boldsymbol{z})^2 \cos^2\theta' \\ &\quad + \left[1 - (\boldsymbol{e} \cdot \boldsymbol{z})^2\right] \sin^2\theta' \cos^2(\epsilon - \phi') \\ &\quad + 2(\boldsymbol{e} \cdot \boldsymbol{z})\left[1 - (\boldsymbol{e} \cdot \boldsymbol{z})^2\right]^{1/2} \\ &\quad \times \cos\theta' \sin\theta' \cos(\epsilon - \phi')\end{aligned} \tag{8}$$

We expand eq. (5) using the identities of eqs. (7) and (8), replace ϕ' by $\phi + \delta$, and observe that all experimentally realizable distributions are cylindrically symmetric and thus are independent of ϕ. Then

$$I = 3I_0\left[(\boldsymbol{a} \cdot \boldsymbol{z})^2(\boldsymbol{e} \cdot \boldsymbol{z})^2\langle\cos^2\theta \cos^2\theta'\rangle\right. \tag{9a}$$

$$+\tfrac{1}{2}(\boldsymbol{a}\cdot\boldsymbol{z})^2\left[1-(\boldsymbol{e}\cdot\boldsymbol{z})^2\right]\langle\cos^2\theta\,\sin^2\theta'\rangle \quad (9b)$$

$$+\tfrac{1}{2}\left[1-(\boldsymbol{a}\cdot\boldsymbol{z})^2\right](\boldsymbol{e}\cdot\boldsymbol{z})^2\langle\sin^2\theta\,\cos^2\theta'\rangle \quad (9c)$$

$$+\tfrac{1}{8}\left[1-(\boldsymbol{a}\cdot\boldsymbol{z})^2\right]\left[1-(\boldsymbol{e}\cdot\boldsymbol{z})^2\right]$$
$$\times\langle\sin^2\theta\,\sin^2\theta'(1+2\cos^2(\epsilon-\delta))\rangle \quad (9d)$$

$$+2(\boldsymbol{a}\cdot\boldsymbol{z})\left[1-(\boldsymbol{a}\cdot\boldsymbol{z})^2\right]^{1/2}$$
$$\times(\boldsymbol{e}\cdot\boldsymbol{z})\left[1-(\boldsymbol{e}\cdot\boldsymbol{z})^2\right]^{1/2}$$
$$\times\langle\cos\theta\,\sin\theta\,\cos\theta'\,\sin\theta'\,\cos(\epsilon-\delta)\rangle\Big\} \quad (9e)$$

Whenever either the probe or emission polarizations are parallel or perpendicular to the pump beam polarization, the term labeled in (9e) vanishes as has been observed by Wegener [25]. The first three terms can be observed independently in both the 90° geometry and the microscope geometry when $\alpha=0$ and $\xi=0$, $\alpha=0$ and $\xi=\pi/2$, and $\alpha=\pi/2$ and $\xi=0$ respectively. The remaining terms become zero for these orientations. For convenience, we describe each of these signals with respect to the polarization of the probe beam and emission polarizer required to isolate them, the pump beam always assumed being z-polarized. Thus, we designate I_{ZZ} as the signal obtained when the probe beam and emission polarizer are both z-polarized. This isolates the term labeled (9a). Likewise, I_{ZY} represents the term labeled (9b) and I_{YZ} the (9c) term. The term labeled (9d) is really a superposition of two observable signals that arise when $\alpha=\pi/2$ and $\xi=\pi/2$. Different azimuthal angles between $\boldsymbol{a}$ and $\boldsymbol{e}$ give rise to two important cases. These are designated as I_{YY} and I_{YX}. The I_{YY} case is when $\boldsymbol{a}$ is colinear with $\boldsymbol{e}$.

$$I_{YY}=\tfrac{3}{8}I_0\langle\sin^2\theta\,\sin^2\theta'(1+2\cos^2\delta)\rangle \quad (10)$$

The I_{YX} case is when $\boldsymbol{a}$ is orthogonal to $\boldsymbol{e}$, i.e. $\boldsymbol{e}$ lies along the x-axis.

$$I_{YX}=\tfrac{3}{8}I_0\langle\sin^2\theta\,\sin^2\theta'(1+2\sin^2\delta)\rangle \quad (11)$$

The sum of these signals isolates the (9d) term without the azimuthal angle dependence:

$$I_{YY}+I_{YX}=\tfrac{3}{2}I_0\langle\sin^2\theta\,\sin^2\theta'\rangle \quad (12)$$

2.2. Solution for 90° geometry

All five signals I_{ZZ}, I_{ZY}, I_{YZ}, I_{YY} and I_{YX} are accessible experimentally in a 90° instrumental geometry. Therefore, we can define signals $E_{\parallel}$ and $E_{\perp}$ representing the total emitted light polarized parallel and perpendicular, respectively, to the z-axis by combining the three signals with the desired emission polarization but excited by the three orthogonal probe polarizations. These sums thus reflect emission from *all* chromophores, independent of the distribution of their absorption dipoles. In particular

$$E_{\parallel}=I_{ZZ}+2I_{YZ} \quad (13)$$

and

$$E_{\perp}=I_{ZY}+I_{YY}+I_{YX} \quad (14)$$

From these we can write the emission anisotropy r_e as

$$r_e=(\Delta E_{\parallel}-\Delta E_{\perp})/s \quad (15)$$

where Δ represents the difference between the predepletion intensity and the intensity at time t for the indicated polarizations. The intensity function s, the total number of excited (triplet) state molecules, is given by

$$s=\Delta E_{\parallel}+2\Delta E_{\perp} \quad (16)$$

Similarly for the absorption anisotropy r_a

$$A_{\parallel}=I_{ZZ}+2I_{ZY} \quad (17)$$

and

$$A_{\perp}=I_{YZ}+I_{YY}+I_{YX} \quad (18)$$

from which we can write

$$r_a=(\Delta A_{\parallel}-\Delta A_{\perp})/s \quad (19)$$

where

$$s=\Delta A_{\parallel}+2\Delta A_{\perp} \quad (20)$$

Inspection shows the definitions of s in eqs. (16) and (20) to be equivalent. This is necessarily the case since s is determined solely by the population of excited state molecules.

The evaluation of either anisotropy function by this method requires five measurements using the orthogonal polarization orientations accessible in the 90° geometry. However, a more efficient approach for obtaining these functions has been described by Wegener [25] and Wegener and Rigler [26]. This approach uses a magic-angle polarization scheme to observe either the light emitted upon unbiased excitation of all chromophores or light absorption as evidenced by total emission over all polarizations. For example, the parallel component $A_{\parallel}$ of the absorption signal is the depletion observed when the pump and probe beam polarizations are rotated 45° from vertical and the emission polarization is rotated 35.3° from vertical. The signal obtained is actually $\frac{1}{3}A_{\parallel}$ since this signal represents a single intensity measurement whereas those in eqs. (17) and (18) are a summation of three such measurements. The perpendicular component $A_{\perp}$ is the depletion measured when the probe beam is rotated 45° relative to vertical and the other two polarization axes remain as in the $A_{\parallel}$ case. This creates a 90° angle between the pump and probe beam polarizations, a 54.7° angle between the emission and pump beam polarizations, and a 54.7° angle between the emission and probe beam polarizations. The quantity observed is again $\frac{1}{3}A_{\perp}$. In a similar fashion, to observe the parallel emission signal $E_{\parallel}$, the pump and emission polarizations are both vertically aligned, while the probe beam polarization makes an angle of 54.7° relative to vertical. To observe $E_{\perp}$, the pump beam is polarized horizontally, the emission polarizer is rotated to an angle of 45° from vertical, and the probe beam polarization is rotated 35.3° from vertical. This creates a 90° angle between the emission and pump beam polarizations, a 54.7° angle between the probe and pump beam polarizations, and a 54.7° angle between the probe beam and emission polarizations. Depletion measurements in these geometries yield $\frac{1}{3}E_{\parallel}$ and $\frac{1}{3}E_{\perp}$, respectively, and the emission anisotropy can be computed as in eq. (15).

This method for obtaining the anisotropy functions reduces the number of measurements from five, as detailed in equations 13, 14, 17 and 18, to four if both r_a and r_e are to be measured. If either r_a or r_e is to be measured alone, the number of required measurements is further reduced to two. The utility of determining both r_a and r_e was demonstrated by Kinosita et al. [21] who showed that $r_e(0)/r_a(0) = P_2(\cos\lambda)$ where $r_e(0)$ and $r_a(0)$ are the initial emission and absorption anisotropies, respectively, P_2 is the second order Legendre polynomial and λ is the interdipole angle. This provides direct determination of the interdipole angle of the chromophore and this quantity has to be independently known for measurements in the microscope as discussed below.

2.3. Solution for microscope geometry

The microscope case is unique in that all polarization axes lie in a plane. This implies that r_e and r_a cannot be calculated from eqs. (13) and (17) because the I_{YX} signal, which is common to both equations, is not obtainable in the microscope. Likewise, Wegener's method cannot be used because the magic angle geometries necessary to measure $E_{\perp}$ and $A_{\perp}$ are not accessible in a microscope. To circumvent this, we express δ in eq. (9) in terms of the interdipole angle λ, θ, and θ' as

$$\sin\theta \sin\theta' \cos\delta = \cos\lambda - \cos\theta \cos\theta' \qquad (21)$$

to obtain the new relation

$$\begin{aligned} I = 3I_0\Big[\Big\{&(\boldsymbol{a}\cdot\boldsymbol{z})^2(\boldsymbol{e}\cdot\boldsymbol{z})^2 \\ &+\tfrac{1}{4}\left[1-(\boldsymbol{a}\cdot\boldsymbol{z})^2\right]\left[1-(\boldsymbol{e}\cdot\boldsymbol{z})^2\right] \\ &+\tfrac{1}{4}\cos^2\lambda\left[1-(\boldsymbol{a}\cdot\boldsymbol{z})^2\right]\left[1-(\boldsymbol{e}\cdot\boldsymbol{z})^2\right] \\ &-2(\boldsymbol{a}\cdot\boldsymbol{z})\left[1-(\boldsymbol{a}\cdot\boldsymbol{z})^2\right]^{1/2} \\ &\times(\boldsymbol{e}\cdot\boldsymbol{z})\left[1-(\boldsymbol{e}\cdot\boldsymbol{z})^2\right]^{1/2}\Big\}\langle\cos^2\theta\cos^2\theta'\rangle \end{aligned} \qquad (22a)$$

$$\begin{aligned} &+\Big\{\tfrac{1}{2}(\boldsymbol{a}\cdot\boldsymbol{z})^2\left[1-(\boldsymbol{e}\cdot\boldsymbol{z})^2\right] \\ &+\tfrac{1}{4}\cos^2\lambda\left[1-(\boldsymbol{a}\cdot\boldsymbol{z})^2\right]\left[1-(\boldsymbol{e}\cdot\boldsymbol{z})^2\right]\Big\} \\ &\times\langle\cos^2\theta\sin^2\theta'\rangle \end{aligned} \qquad (22b)$$

$$+\left\{\tfrac{1}{2}\left[1-(a\cdot z)^2\right](e\cdot z)^2 + \tfrac{1}{4}\cos^2\lambda\left[1-(a\cdot z)^2\right]\left[1-(e\cdot z)^2\right]\right\} \times\langle\sin^2\theta\cos^2\theta'\rangle \quad (22c)$$

$$+\left\{\tfrac{1}{8}\left[1-(a\cdot z)^2\right]\left[1-(e\cdot z)^2\right] + \tfrac{1}{4}\cos^2\lambda\left[1-(a\cdot z)^2\right]\left[1-(e\cdot z)^2\right]\right\} \times\langle\sin^2\theta\sin^2\theta'\rangle \quad (22d)$$

$$+\left\{2\cos\lambda(a\cdot z)\left[1-(a\cdot z)^2\right]^{1/2} \times(e\cdot z)\left[1-(e\cdot z)^2\right]^{1/2} - \tfrac{1}{2}\cos\lambda\left[1-(a\cdot z)^2\right]^{1/2} \times\left[1-(e\cdot z)^2\right]^{1/2}\right\}\langle\cos\theta\cos\theta'\rangle \quad (22e)$$

The term labeled (22e) contains cross terms in θ and θ' that are not useful in calculating the anisotropy functions. For this reason we wish to eliminate it. To do this, we determine an experimental geometry that causes each of the terms contained in it to cancel. This occurs when both the probe beam and emission polarizer are colinear and at an angle of 63.4° relative to the pump beam. We call this the I_{6363} geometry. Upon calculation and reduction

$$I_{6363} = \tfrac{3}{25}I_0\{-(3-4\cos^2\lambda)\langle\cos^2\theta\cos^2\theta'\rangle + (2+4\cos^2\lambda)\langle\cos^2\theta\sin^2\theta'\rangle + (2+4\cos^2\lambda)\langle\sin^2\theta\cos^2\theta'\rangle + (2+4\cos^2\lambda)\langle\sin^2\theta\sin^2\theta'\rangle\} \quad (23)$$

At this point we are able to write an expression for the microscope-based equivalent of $I_{YY}+I_{YX}$ (cf. eq. 10).

$$I_{YY}+I_{YX} = \frac{25}{(4+8\cos^2\lambda)}I_{6363} + \frac{(3-4\cos^2\lambda)}{(4+8\cos^2\lambda)}I_{ZZ}-I_{ZY}-I_{YZ} \quad (24)$$

Using eqs. (10)–(14), (24), and a value for λ, the interdipole angle, we can write expressions for the parallel and perpendicular components of the emission signal in analogy with eqs. (13) and (14).

$$E_{\parallel} = I_{ZZ}+2I_{YZ} \quad (25)$$

$$E_{\perp} = \frac{25}{(4+8\cos^2\lambda)}I_{6363} + \frac{(3-4\cos^2\lambda)}{(4+8\cos^2\lambda)}I_{ZZ}-I_{YZ} \quad (26)$$

Substitution of the I_{ZY} signal for the I_{YZ} signal in eqs. (25) and (26) produces the absorption parallel and perpendicular components. From these expressions, we can now write the absorption and emission anisotropy and total intensity functions for a microscope-based system.

$$r_a = \left[(\Delta I_{ZZ}+2\Delta I_{ZY}) - \left(\frac{25}{4+8\cos^2\lambda}\Delta I_{6363} + \frac{3-4\cos^2\lambda}{4+8\cos^2\lambda}\Delta I_{ZZ}-\Delta I_{ZY}\right)\right]/s \quad (27)$$

$$r_e = \left[(\Delta I_{ZZ}+2\Delta I_{YZ}) - \left(\frac{25}{4+8\cos^2\lambda}\Delta I_{6363} + \frac{3-4\cos^2\lambda}{4+8\cos^2\lambda}\Delta I_{ZZ}-\Delta I_{YZ}\right)\right]/s \quad (28)$$

$$s = (\Delta I_{ZZ}+2\Delta I_{YZ}) + 2\left(\frac{25}{4+8\cos^2\lambda}\Delta I_{6363} + \frac{3-4\cos^2\lambda}{4+8\cos^2\lambda}\Delta I_{ZZ}-\Delta I_{YZ}\right) \quad (29)$$

Thus, r_a and r_e can each be calculated from three separate fluorescence intensity measurements. If both r_a and r_e are to be calculated, the number of required measurements is increased to four.

3. Experimental

We have constructed an instrument capable of acquiring the signals necessary to calculate true emission and absorption anisotropies in both the 90° and the microscope geometries. This instrument is also capable of performing time-resolved phosphorescence anisotropy (TPA) experiments on cuvet samples.

3.1. Instrumentation

A block diagram of the PFD/TPA with our instrument as used for 90° measurements on cuvet samples is presented in Fig. 2. The probe beam, used only for PFD experiments, consists of the 514 nm line of a Coherent Radiation Innova 90-3 argon ion laser. This laser operates in its vertically polarized TEM_{00} output mode at 500 mW of power. The beam passes first through neutral density filters, a Coherent Radiation 304d acousto-optic modulator, a computer-controlled rotatable half-wave plate and a beam iris. The acoustooptic modulator and iris function as an optical switch serving two purposes. First, the probe beam is switched off at the sample just prior to the end of data acquisition. We treat this period without probe beam as the zero signal level for data analysis purposes. Second, by illuminating the sample only during data acquisition period, we reduce chromophore photobleaching. Next, the probe beam is expanded by a double beam expanding telescope to approximately the same size as the pump beam and is directed onto the sample.

The pump beam used for PFD experiments is the frequency-doubled 532 nm output from a Spectra Physics DCR-11 Nd:YAG pulse laser fitted with a prism harmonic separator and with optics providing a pseudo-Gaussian beam profile. This beam also serves as the excitation source for time-resolved phosphorescence anisotropy exper-

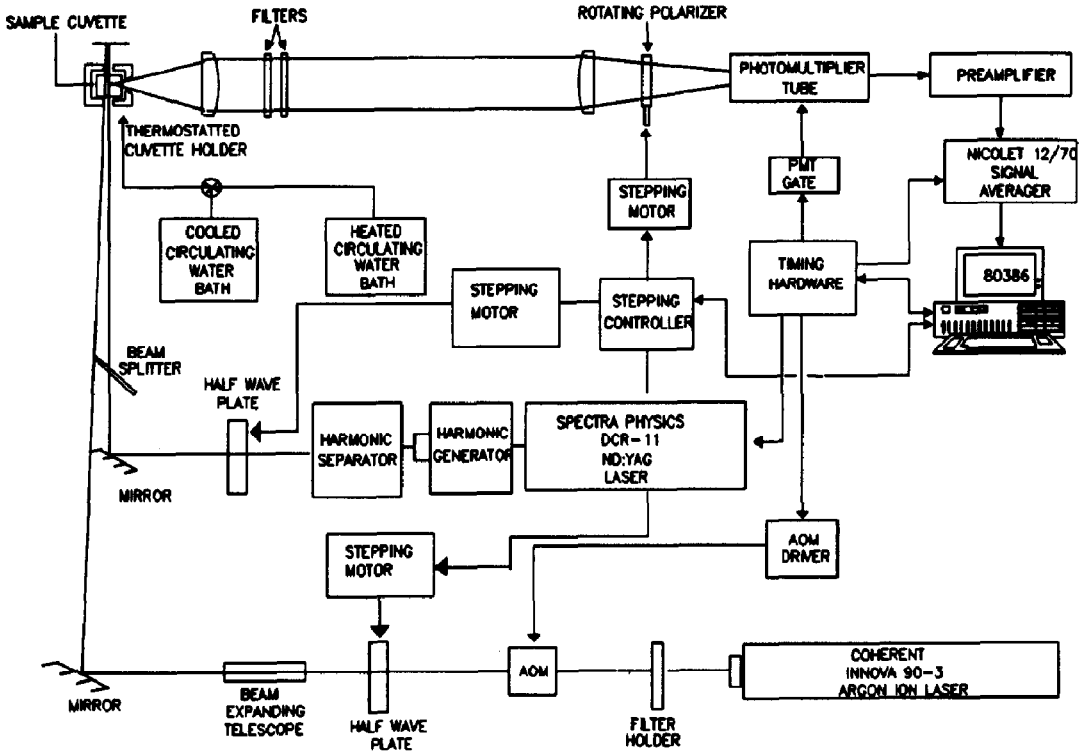

Fig. 2. Block diagram of cuvet PFD/TPA instrument. See text for detailed explanations of the functions of the various components.

iments. The beam passes through a rotatable half-wave plate, which is computer controlled, and is directed onto the sample colinearly with the probe beam. The laser is operated at 10 Hz with a vertically polarized TEM_{00} output of 0.1–1.5 mJ at the sample cuvet. The sample cuvet is held in a thermostated holder mounted on a breadboard adjacent to the main laser table. Fluorescence emission is collected along an axis 90° to the probe and pump beam axis. In PFD experiments, fluorescence passes through a concentrated sodium dichromate solution, a KV550 longpass filter, and 600 nm shortpass filter to eliminate spurious signal due to laser beam scatter, Raman emission or sample phosphorescence. Emitted light is passed through a computer-controlled rotatable polarizer and is focussed onto a Thorn EMI 9816A photomultiplier tube. The photomultiplier is equipped with fast gating electronics [30,31] with a rise and fall time of about 40 ns. This allows us to resume signal acquisition within one datum after the pump pulse. The photomultiplier tube output is amplified by a 100 MHz bandwidth, 100 $V/\mu A$ current-to-voltage converter and fed into a Tektronics model 453 oscilloscope. The vertical preamplifier output of the oscilloscope is amplified about 3.5 × by a 70 MHz bandwidth buffer amplifier to drive the 0.5V input of a Nicolet 12/70 signal-averager. Data are digitized at rates of 500 kHz to 20 MHz with 8-bit precision and averaged in the Nicolet's 20-bit memory. After acquisition is complete, the data are downloaded to an 80386 microcomputer for data analysis and storage. System timing is controlled by a timing computer based on the Metrabyte CTM-05 counter-timer and configured to provide ten independent timing channels [32]. Two recent modifications of the optical system are worthy of mention. The Gaussian output optics of the DCR-11 laser have proved essential in satisfactorily matching the Nd:YAG pump and argon probe beam profiles at the sample, a quantity that cuvet measurements have shown to be critical. The other point concerns stability of Nd:YAG laser pulses. Measurements showed considerable downward drift in pulse intensities with a typical 128-pulse sequence. This apparently arises from resonator cooling between, and heating during, pulse trains. By firing the flash lamp synchronously throughout the experiment, but operating the Q-switch only when a pump pulse is desired, an enormous improvement in pulse is desired, an enormous improvement in pulse stability has been realized.

The microscope-based system is essentially identical to that described above, but with the cuvet holder, collection optics and detector replaced by a Zeiss Universal fluorescence microscope as described previously [14,29]. The principal difference in microscope-related components relative to the previous microscope system is that a rotatable emission polarizer has been placed between the microscope photometer and a fiberoptic bundle leading to the photomultiplier tube which is now mounted on the laser table.

3.2. Data collection and analysis

3.2.1. Data collection

Samples typically consist of eosin isothiocyanate-conjugated proteins rotating in cell membranes or in viscous solutions. Samples are deoxygenated by argon purging or by enzymic oxygen scavenging [33] to provide adequately long triplet lifetimes. Data collection is controlled by an 80386 microcomputer. An experiment involves collecting data in two to four experimental configurations characterized by the orientations of the pump and probe half-wave plates and the emission polarizer. The signal averager is set to average into a specific block of memory, the three rotators are moved to the desired configuration and 128 recovery traces are averaged. A recovery trace includes a number of points before the depletion pulse, the period of fluorescence recovery and a final number of points during which the probe beam is gated off. The 100 ms between laser pulses allows for complete decay of all triplets. The active Nicolet memory region is then moved and 128 background traces with probe beam but without pump pulses are recorded. This sequence is repeated for the other necessary orientations to constitute one basic experimental cycle. Experimental cycles are repeated until averaged signals displayed on the Nicolet 12/70 exhibit adequate signal-to-noise ratios. Data are

then downloaded to the host microprocessor for analysis. It should be pointed out that, because this is a depletion experiment, the background traces are fully as important as the recovery traces and so must be obtained with the same statistical confidence.

3.2.2. Cuvet PFD data treatment

The realities of the optical system guarantee that the intensities of pump pulses and probe beam will vary according to the pump and probe polarizations, respectively, and that that the detector will exhibit different sensitivity according the the setting of the emission polarizer. Satisfactory results in PFD experiments depend upon proper compensation for *all* these factors in *each* experiment.

First, for each trace the average intensity during the probe-off period at the end of the acquisition cycle (see Instrumentation section) is subtracted from the average predepletion intensity to yield an amplitude proportional to the product of the probe intensity and detector sensitivity. Next, each trace is scaled to make its amplitude agree with that of the data trace of one particular configuration. Then data traces are subtracted, point for point, from their respective background traces to yield corrected depletion signals. This operation yields depletion signals prefixed by a "Δ". Next, using emission anisotropy as an example, the total intensity and anisotropy functions are calculated by

$$s = \Delta E_{\parallel} + g2\Delta E_{\perp} \tag{30}$$

$$r_e = (\Delta E_{\parallel} - g\Delta E_{\perp})/s \tag{31}$$

Here g is an instrumental constant close to unity which reflects primarily the polarization dependence of pump pulse intensities. This quantity is evaluated daily from measurements on dye samples having long triplet lifetimes but short rotational correlation times and is selected so as to make r_e for such samples equal to zero at long times. Cuvet PFD data for absorption anisotropies are treated in the same manner except that the signals for $A_{\parallel}$ and $A_{\perp}$ were used in place of those for $E_{\parallel}$ and $E_{\perp}$.

3.2.3. Microscope PFD data treatment

Background scaling and subtraction are performed as in cuvet PFD. For emission microscope PFD data, s and r are calculated using

$$s = (\Delta I_{ZZ} + 2\Delta I_{YZ}) + 2f\left(\frac{25}{4 + 8\cos^2\lambda}\Delta I_{6363} + \frac{3 - 4\cos^2\lambda}{4 + 8\cos^2\lambda}\Delta I_{ZZ} - \Delta I_{YZ}\right) \tag{32}$$

$$r_e = \left[(\Delta I_{ZZ} + 2\Delta I_{YZ}) - f\left(\frac{25}{4 + 8\cos^2\lambda}\Delta I_{6363} + \frac{3 - 4\cos^2\lambda}{4 + 8\cos^2\lambda}\Delta I_{ZZ} - \Delta I_{YZ}\right)\right]/s \tag{33}$$

where f is an instrumental constant and λ is the interdipole angle (see section 2 for the discussion leading to eqs. 32 and 33). The constant f, and its analog for absorption anisotropy, is evaluated from measurements on dye solutions as described above. Optionally, corrections can also be applied to individual ΔI signals to correct for the polarization dependences of the pump beam intensity, probe beam intensity and detector sensitivity [32]. The absorption intensity and anisotropy functions are calculated in the same manner with the exception that the I_{ZY} signal was used instead of the I_{YZ} signal.

3.2.4. Analysis of intensity and anisotropy functions

In our experiments, $s(t)$ is fitted to a multiexponential decay model to obtain the triplet lifetime(s) of the fluorescent probe and the amplitude(s) of their decay. For most xanthine dyes including eosin, two or three lifetimes are required to give a satisfactory fit. Results from the lifetime analysis are then used to weight points in a non-linear least squares fit of the anisotropy decay data.

Statistical considerations show that the error

σ_r in anisotropies obtained in depletion measurements is given by

$$\sigma_r = 2\sqrt{p}/s \tag{34}$$

where p, assumed to be constant, is the number of photoelectron packets detected per channel and s is described in eqs. (30) and (32) for cuvet and microscope signals, respectively. It can be seen that depletion anisotropies are not as well determined at long times as are those obtained from phosphorescence emission since uncertainties in the latter quantities are given by

$$\sigma_r = \sqrt{2}/\sqrt{3s} \tag{35}$$

Using a weighting factor $w_i = 1/\sigma_r^2$ permits anisotropy decay data to be properly analyzed according to a single- or multi-exponential decay models. The single exponential model is usually adequate for cellular data

$$r(t) = r_\infty + (r_0 - r_\infty)\exp(-t/\phi) \tag{36}$$

Fitting $r(t)$ to eq. (36) yields the initial anisotropy value r_0, the limiting anisotropy value r_∞ the rotational correlation time ϕ, and statistical uncertainties in these quantities.

4. Results and discussion

Samples consisting of eosin isothiocyanate (EITC)-conjugated bovine serum albumin (BSA) in glycerol–water solutions were examined to obtain time-dependent absorption and emission anisotropy functions. Typical conjugation ratios were 1–2 mol EITC per mol protein [33]. Samples were examined in both cuvet and microscope configurations under various experimental conditions. The results of these studies are presented below.

4.1. Cuvet results

Figure 3 shows raw data obtained from a typical cuvet absorption PFD experiment. These data

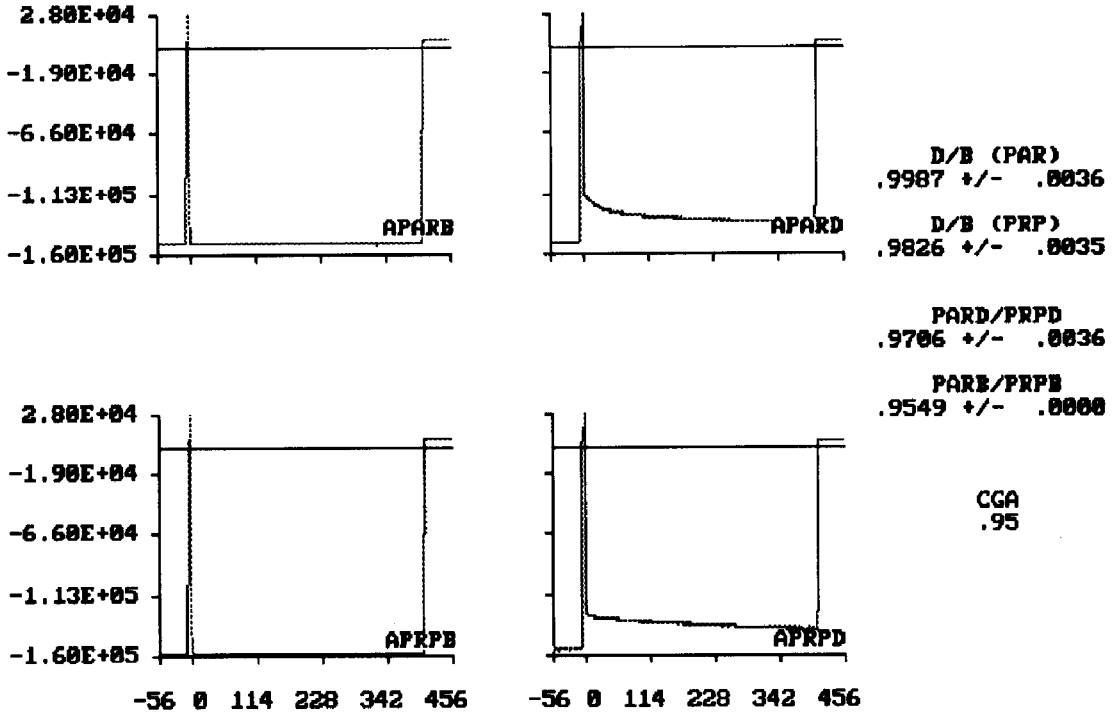

Fig. 3. Typical raw data from cuvet absorption PFD experiment. The sample was 100 nM EITC-BSA in 90% glycerol at 15°C. The y-axes are fluorescence intensities in arbitrary units while the x-axes are times in microseconds. The upper two plots are parallel background and data traces, from left to right. The lower two plots are perpendicular background and data traces, from left to right. "D/B (PAR)" and "D/B (PRP)" are the data-to-background predepletion intensity ratios for the parallel and perpendicular traces, respectively. "PARD/PRPD" and "PARB/PRPB" are the parallel-to-perpendicular predepletion intensity ratios for the data and background traces, respectively. "CGA" is the g-factor used in calculating the intensity and anisotropy functions.

were obtained from a 100 nM sample of eosin isothiocyanate-conjugated bovine serum albumin in 90% glycerol at 15°C. The photomultiplier tube photocurrent is fed directly into the oscilloscope preamplifier and appears as a negative-going signal. The upper two plots of the figure are the parallel background signal (left) and data signals (right). The lower two plots are the perpendicular background and data signals. The "D/B (PAR)" and "D/B (PRP)" values presented at the far right of the figure are the data trace average predepletion intensities divided by the corresponding background trace average predepletion intensities. "D/B (PAR)" represents the parallel data-to-background ratio and "D/B (PRP)" is the perpendicular data-to-background ratio. These values are used to adjust the magnitude of the background signals to the magnitude of the recovery signals. As stated in the data analysis section, this eliminates difficulties arising from a variety of sources including irreversible sample photobleaching. The "PARD/PRPD" and "PARB/PRPB" values presented in the figure are used to properly scale the perpendicular data and background signals to the corresponding parallel signals. This compensates for variations in probe beam intensity in different polarizations arising from instrumental optics. The "PARD/PRPD" value is the intensity ratio of the parallel data signal relative to the perpendicular data signal. The "PARB/PRPB" value is a similar ratio for the parallel and perpendicular background signals. "CGA" at the lower right of Fig. 3 is the instrumental g-factor described in eqs. (30) and (31). This value accounts for differences in pump beam intensities in different polarizations.

Figure 4 illustrates the corrected absorption depletion data corresponding to the raw data in Fig. 3. The parallel absorption depletion signal is the higher of the two and the perpendicular depletion signal is the lower. Differences in the initial regions result from the orientational anisotropy of ground-state depleted molecules produced by the polarized pump beam. Over time, the molecules randomize rotationally in solution and, eventually, the sample becomes orientationally isotropic with respect to the ground

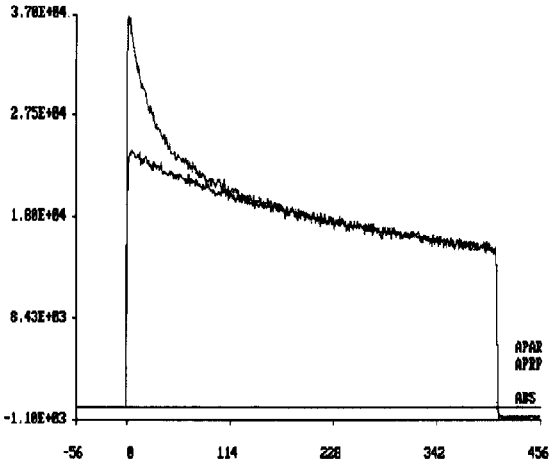

Fig. 4. Total depletion signals from a cuvet absorption PFD experiment. The sample was 100 nM EITC-BSA in 90% glycerol at 15°C. The y-axis is depletion intensity in arbitrary units while the x-axis is time in microseconds. The upper curve is parallel depletion $\Delta A_{\parallel}$ and the lower curve is the perpendicular depletion $\Delta A_{\perp}$.

state depleted molecules. At this point, the parallel and perpendicular signals coincide as seen in the latter portions of the figure.

The time-dependent absorption anisotropy decay implies by this figure is explicit depicted in Fig. 5. The upper plot contains the absorption total intensity function and the lower plot illustrates the absorption anisotropy function, both calculated from the data in Fig. 3. Results from non-linear least squares fitting of these curves are displayed to the right of the plots. Total intensity data were modeled using a two-exponential decay fitting function with constant baseline. From this we obtained the baseline amplitude, the first pre-exponential factor, the first exponential time constant, the second pre-exponential factor, and the second exponential time constant. These parameters are displayed immediately to the right of the total emission plots and are labeled "CONST", "AMP1", "TK1", "AMP2" and "TK2", respectively. Also displayed in the figures are the standard deviations of the derived parameters and the figure of merit of the fit "CHI2". When data are obtained via single photon counting, this quantity is the reduced χ^2 for the fit; but, as here when data are recorded by digitization of currents signals, it is simply an arbitrary

Table 1

Cuvet PFD measurement of BSA rotation [a]

Temp. (°C)	r_a (0) [b]	ϕ_a (μs) [c]	r_e (0) [d]	ϕ_e (μs) [e]	λ (deg) [f]
6.7	0.178±0.073	173.4 ±12.4	0.121±0.006	203.2 ±43.9	27.5±0.2
16.9	0.163±0.073	61.85± 8.17	0.116±0.020	69.45± 4.30	26.0±0.3
28.3	0.156±0.027	28.70± 2.40	0.118±0.018	31.35± 0.22	23.8±0.2

[a] Sample consisted of 100 nM EITC-BSA in 90% glycerol.
[b] Initial absorption anisotropy calculated from eq. (19).
[c] Rotational correlation time determined from absorption anisotropy decay.
[d] Initial emission anisotropy calculated from eq. (15).
[e] Rotational correlation time determined from emission anisotropy decay.
[f] Angle between μ_a and μ_e.

measure of merit. The anisotropy decay was fitted to eq. (36). Parameters derived from this fit are the initial anisotropy "R(INIT)", the final anisotropy "R(INF)" and the rotational correlation time "RCT". These values and their associated standard deviations are displayed in Fig. 5 directly to the right of the anisotropy plot. The figure of merit "CHI2" for this fit should also be displayed but, due to a programming error, is not.

A summary of cuvet PFD results obtained from samples containing 100 n*M* EITC-BSA in 90% glycerol at 6.7, 16.9, and 28.3°C is presented in Table 1. This Table contains initial absorption anisotropies, the rotational correlation time deduced from absorption anisotropy decay and the estimated errors in these quantities. Similar information is provided for emission anisotropy measurements. In all cases the limiting anisotropies were statistically indistinguishable from zero. Finally, the interdipole angle is estimated from comparison of absorption and emission results. This latter quantity, averaging 26°, agrees well with values reported for other xanthine dyes.

4.2. Microscope PFD results

The limiting sensitivity of the microscope PFD method is shown by results obtained from samples containing 500 n*M* EITC-BSA in 90% glycerol at 15, 20, and 25°C and presented in Table 2. A value of 26° was assumed for the interdipole angle as estimated from cuvet PFD measurements. The Table contains the same quantities reported in Table 1 except that the interdipole angle is not calculated. The rotational correlation times at various temperatures obtained by this method are in good agreement with those obtained using cuvet PFD (see Table 1). This is despite the extremely small number of fluorophores examined in each measurement. The

Table 2

Microscope PFD measurement of BSA rotation [a]

Temp. (°C)	r_a (0) [b]	ϕ_a (μs) Uc	r_e (0) [d]	ϕ_e (μs) [e]
15	0.078±0.013	86.59±21.25	0.104±0.012	110.8 ±21.8
20	0.091±0.003	45.94± 1.10	0.096±0.012	67.00± 7.09
25	0.047±0.016	30.52±14.75	0.061±0.016	32.92± 7.83

[a] Sample consisted of 500 n*M* EITC-BSA in 90% glycerol. This represents only about 2,000,000 chromophores being examined and was chosen to illustrate te limiting sensitivity of the method. A value of 26° was assumed for λ.
[b] Initial absorption anisotropy calculated from eq. (27).
[c] Rotational correlation time determined from absorption anisotropy decay.
[d] Initial emission anisotropy calculated from eq. (28).
[e] Rotational correlation time determined from emission anisotropy decay.

agreement of the microscope initial anisotropies with those obtained from cuvet measurements is not so satisfactory and this arises simply from the very small number of chromophores being examined in these particular microscope measurements. With more concentrated samples in the microscope, good agreement with cuvet results is obtained. From the sample concentration, sample thickness, beam diameter on the microscope stage and number of fluorochromes per protein, one calculates that about 2,000,000 chromophores are interrogated in each measurement from which a usable anisotropy decay curve is obtained. This is roughly equivalent to the number of fluorochromes on the surface of five 2H3 cells bearing EITC-conjugated IgE. From these data we conclude that we are very close to obtaining useful rotation measurements of a particular protein located on a single cell.

4.3. Preliminary cellular results

Before the current methods of data acquisition and analysis were available, we performed preliminary cuvet PFD studies on rat 2H3 mast cells labeled with EITC-derivatized rat IgE [20]. Unfortunately, present knowledge shows that data obtained at that time cannot be analyzed to obtain quantitatively meaningful anisotropies. None the less, results of this study show qualitatively that signals adequate to measure protein rotational correlation times could be obtained by PFD observation of approximately 10^4 cells in the beam path. The time required for such measurements was the same as required for time-resolved phosphorescence anisotropy measurements and less than 1/150 the time necessary for comparable single cell PFD measurements. Cuvet PFD studies of membrane protein rotation in a variety of cellular systems are now underway using the techniques described in this paper.

4.4. Other aspects of instrumental characterization

Measurements on earlier instruments were limited to rotational correlation times exceeding 10 μs. This system, with its fast PMT gate and low jitter timing circuitry [30,31], permits the

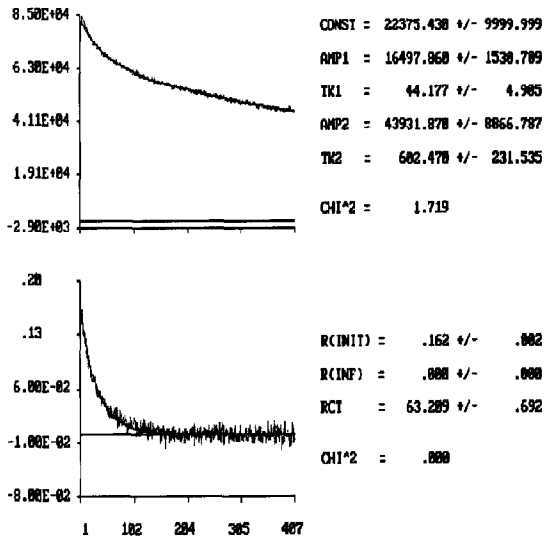

Fig. 5. Fitted intensity and anisotropy functions from a cuvet absorption PFD experiment. The sample contained 100 nM EITC-BSA in 90% glycerol at 15°C. The y-axis are intensities in arbitrary units while the x-axes are times in microseconds. The upper plot is the fitted absorption intensity function. The lower plot is the fitted absorption anisotropy. See text for explanation of the fitting parameters displayed to the right of the plots.

measurement of faster rotational correlation times than were previously obtainable. We have tested this via time-resolved phosphorescence anisotropy measurement of erythrosin isothiocyanate-conjugated bovine serum albumin rotation in glycerol solutions of varying viscosity [20]. As the solvent viscosity was reduced from 2500 to 15 cP, the corresponding protein rotational correlation times decreased from 316 to 2.5 μs, respectively. In more recent experiments rotational correlation times as low as 500 ns have been measured. This ability to measure faster rotational correlation times now permits rotational motion studies of membrane proteins, such as Major Histocompatibility Complex Class II antigens, which have small in-membrane domains. Faster digitization capabilities and more sophisticated gating strategies will be necessary to measure faster rotational dynamics. However, measurement of such fast rotation seems of limited practical importance since all integral membrane proteins we have examined to date have exhibited

rotational correlation time within the time scale currently accessible.

Theoretically, PFD measurements should be at least 100 times more sensitive than analogous TPA procedures. We are trying to realize this full sensitivity. We can currently measure anisotropy decay via PFD in cuvet samples containing 50 p*M* EITC. This is about 20 times more sensitive than corresponding time-resolved phosphorescence anisotropy measurements. The major factor reducing PFD sensitivity at low concentrations is gating transients of the same magnitude as the fluorescence signal.

5. Conclusions

Existing techniques such as time-resolved phosphorescence anisotropy are often adequate to measure protein rotation on large samples of cells. However, if the cells to be examined must be selected from within a large population based on some morphological criterion, then microscope-based methods with sensitivity adequate to single cell measurements must be employed. As stated earlier, the only such method currently available is PFD. In this paper we extend existing theory to permit calculation of well-defined anisotropy functions from microscopic PFD observations. Our results demonstrate that knowledge of the interdipole angle, along with three separate fluorescence measurements, serve to determine a true absorption anisotropy or a true emission anisotropy. This number is increased to four independent measurements if both absorption and emission anisotropies are to be calculated. This corresponds with Wegener's [25] theory predicting that four independent measurements are required to completely describe the rotational behavior of a sample when measured using other experimental geometries.

We previously constructed an instrument capable of measuring by PFD membrane protein rotational diffusion on single cells [14,37]. This instrument can now perform both PFD and TPA measurements on cell suspensions contained in cuvets as well as microscope-based PFD on single cells. A single instrument able to gather data by all three methods permits direct comparisons of the relative advantages and disadvantages of each technique. From our preliminary studies, it is clear that the cuvet measurements provide greatly increased signal-to-noise ratios when compared to single cell measurements. On the other hand, the ability to examine hand-selected cells using the microscope-based system, as opposed to large ensembles of cells in the cuvet-based system, has distinct advantages for cellular studies.

Acknowledgement

This work was supported in part by NIH grants AI-21873 and AI-26621 (B.G.B.) and HD-23236 (D.A.R.).

Glossary

$\boldsymbol{a}$	Probe beam polarization vector
α	Angle between probe polarization and z-axis
$\boldsymbol{a}\cdot\boldsymbol{z}$	$\cos\alpha$
$[1-(\boldsymbol{a}\cdot\boldsymbol{z})^2]^{1/2}$	$\sin\alpha$
$\boldsymbol{e}$	Emission polarizer polarization axis
ξ	Angle between emission polarization and z-axis
$\boldsymbol{e}\cdot\boldsymbol{z}$	$\cos\xi$
$[1-(\boldsymbol{e}\cdot\boldsymbol{z})^2]^{1/2}$	$\sin\xi$
ϵ	Azimuthal angle between probe beam and emission polarization vectors
μ_a	Absorption transition dipole
θ	Polar angle between absorption dipole and z-axis
ϕ	zimuthal angle between probe beam polarization and absorption dipole
μ_e	Emission transition dipole

θ'	Polar angle between emission dipole and z-axis
ϕ'	Azimuthal angle between probe beam polarization and emission dipole
λ	Interdipole angle between μ_a and μ_e
δ	Azimuthal angle between absorption and emission dipoles
$P(\theta, \phi, \theta', \phi')$	Absorption and emission dipole distribution function
$(a \cdot \mu_a)^2$	Magnitude of projection of probe beam polarization on absorption dipole
$(e \cdot \mu_e)^2$	Magnitude of projection of emission polarizer on emission dipole
$B/3$	Total fractional ground state depletion
P_0, P_2	Zero and second order Legendre polynomials
S	Ground state chromophore distribution function
I_p	Intensity of depletion pulse
λ_p	Wavelength of light of depletion pulse
ϵ_M^p	Molar absorptivity for pump beam
ϵ_M^a	Molar absorptivity for probe beam
Φ_t	Quantum yield for triplet formation
h	Planck's constant
c	Speed of light
N	Avogadro's number
Δt	Duration of depletion pulse
$\langle \cdot \rangle$	Average value
I_0	Pre-depletion fluorescence intensity
I_a	Intensity of probe beam
Φ_f	Quantum yield for fluorescence
E_f	Detector efficiency
λ_e	Fluorescence emission wavelength
n	Total number of chromophores illuminated
I_{ZZ}	Signal with probe parallel to z-axis and emission parallel to z-axis
I_{ZY}	Signal with probe parallel to z-axis and emission parallel to y-axis
I_{YZ}	Signal with probe parallel to y-axis and emission parallel to z-axis
I_{YX}	Signal with probe parallel to y-axis and emission parallel to x-axis
I_{YY}	Signal with probe parallel to y-axis and emission parallel to y-axis
I_{6363}	Signal with probe parallel to emission and both 63° from z-axis
ΔI	Difference between predepletion and time-dependent intensities
$A_\parallel$	Parallel absorption signal
$A_\perp$	Perpendicular absorption signal
$E_\parallel$	Parallel emission signal
$E_\perp$	Perpendicular emission signal
r_a	Absorption anisotropy function
r_e	Emission anisotropy function
s	Intensity function

References

1 D.A. Axelrod, J. Membr. Biol. 75 (1983) 1–10.
2 G.M. Edelman, Science 192 (1976) 218–226.
3 M. Edidin, Annu. Rev. Biophys. Bioeng. 3 (1974) 179–201.
4 D. Chapman and C.J. Restall, Biochem. Soc. Symp. 46 (1979) 139–154.
5 F. Jähnig, Proc. Natl. Acad. Sci. USA 76 (1981) 6361–6365.

6 R.J. Cherry, Meth. Enzymol. 54 (1978) 47–61.
7 R.J. Cherry, Biochim. Biophys. Acta 559 (1979) 289–327.
8 R. Greinhert, H. Stark, A. Steir and A. Weller, J. Biochem. Biophys. Meth. 1 (1979) 77–83.
9 R. Austin, S. Chan and T. Jovin, Proc. Natl. Acad.Sci. USA, 76 (1979) 5650–5654.
10 R. Cherry, A. Cogoli, M. Oppliger, G. Schneider and G. Semenza, Biochemistry 15 (1976) 3653–3656.
11 P. Johnson and P.B. Garland, FEBS Lett. 132(2) (1981) 252–256.
12 P. Garland and P. Johnson, Rotational diffusion of membrane proteins optical methods, in: Enzymes of biological membranes, vol. 1, 2nd edn., ed. A.N. Martonosi (Plenum Press, New York, 1985) 421–439.
13 T.M. Yoshida, F. Zarrin and B.G. Barisas, Biophys. J. 54 (1988) 277–288.
14 B.G. Barisas, N.A. Rahman, T.M. Yoshida and D.A. Roess, SPIE Proc. 1204 (1989) 765–774.
15 T.M. Yoshida and B.G. Barisas, Biophys. J. 50 (1986) 41–53.
16 B.G. Barisas, N.A. Rahman, T.R. Londo, J.R. Herman and D.R. Roess, SPIE Proc. 1432 (1991) 52–63.
17 P.B. Garland and C.H. Moore, Biochem. J. 183 (1979) 561–575.
18 F. Perrin, J. Phys. 12 (1926) 390–401.
19 L.M. Smith, R.M. Weiss and H.M. McConnell, Biophys. J. 36 (1981) 73–91.
20 D.A. Axelrod, Biophys. J. 26 (1979) 557–573.
21 K. Kinosita, S. Kawato and A. Ikegami, Biophys. J. 20 (1977) 289–305.
22 G. Weber, Biochem. 51 (1951) 145–167.
23 M. Ehrenberg and R. Rigler, Chem. Phys. Lett. 14(5) (1972) 539–544.
24 A. Szabo, J. Chem. Phys. 81(1) (1984) 150–167.
25 W. Wegener, Biophys. J. 46 (1984) 795–803.
26 W. Wegener and R. Rigler, Biophys. J. 46 (1984) 787–793.
27 S.R. Aragon and R. Pecora, Biopolymers 14 (1975) 119–138.
28 S.R. Aragon and R. Pecora, J. Chem. Phys. 64(4) (1976) 1791–1803.
29 T.R. Londo and B.G. Barisas, SPIE Proc. 1640 (1992) 309–318.
30 T.M. Yoshida, T. Jovin and B.G. Barisas, 60 (1989) 2924–2928.
31 J.R. Herman, T.R. Londo, N.A. Rahman and B.G. Barisas, Rev. Sci. Instrum. 63 (1992) 5454–5458.
32 T.R. Londo, Theoretical and instrumental developments in the measurement of integral membrane protein dynamics, Ph.D. Dissertation, Colorado State University (1992) 486 pp.
33 N. Rahman, I. Pecht, D.A. Roess, B.G. Barisas, Biophys. J. 161 (1992) 334–343.
34 R. Zidovetzki, M. Bartholdi, D. Arndt-Jovin and T. Jovin, Biochemistry 25 (1986) 4397–4401.